J. Fluid Mech. (1987), *vol.* 178, *pp.* 345–365
Printed in Great Britain

Numerical study of ribbon-induced transition in Blasius flow

By PHILIPPE R. SPALART
NASA Ames Research Center, Moffett Field, CA 94035, USA

AND KYUNG-SOO YANG
Stanford University, Stanford, CA 94305, USA

(Received 30 December 1985 and in revised form 1 October 1986)

The early three-dimensional stages of transition in the Blasius boundary layer are studied by numerical solution of the Navier–Stokes equations. A finite-amplitude two-dimensional wave and low-amplitude three-dimensional random disturbances are introduced. Rapid amplification of the three-dimensional components is observed and leads to transition. For intermediate amplitudes of the two-dimensional wave the breakdown is of subharmonic type, and the dominant spanwise wavenumber increases with the amplitude. For high amplitudes the energy of the fundamental mode is comparable to the energy of the subharmonic mode, but never dominates it; the breakdown is of mixed type. Visualizations, energy histories, and spectra are presented. The sensitivity of the results to various physical and numerical parameters is studied. The agreement with experimental and theoretical results is discussed.

1. Introduction

Our ability to understand, predict, and control the transition of fluid flows from laminar to turbulent states is far from satisfactory, in spite of decades of effort. Transition is very sensitive both to the exact shape of the basic laminar flow and to the detailed characteristics (amplitude, spectrum, etc.) of the disturbances, whether they are associated with the stream or with the surface. Natural transition is very intermittent and thus is difficult to measure. The control of transition would allow significant improvements in many applications; for instance, reduced skin-friction drag or higher lift coefficients for wings, or enhanced mixing for combustion and chemical reactions.

Several stages can be distinguished as one observes the transition of a boundary layer, starting from upstream. At first the disturbances, within the basic laminar flow, are small enough to be described by the linear Orr–Sommerfeld equation (Schlichting 1979). The 'linear' behaviour of single two-dimensional and oblique Tollmien–Schlichting (TS) waves is well understood, but in practice numerous waves compete and grow simultaneously. The slow thickening of the boundary layer adds to the complexity of the situation. In any case, linearized theory is insufficient to predict transition, because it fails to predict the large growth rates that are observed. The linear stage is followed by an 'early nonlinear' stage during which nonlinear effects become significant, but the disturbances are still rather weak and the flow is still smooth. The nonlinear effects are revealed by much larger growth rates of some of the disturbances, which are invariably three-dimensional. Two-dimensional nonlinear effects, such as the saturation of a TS wave, are benign and are unable to

induce transition, probably because of the absence of vortex stretching. Finally, there is a strongly nonlinear stage which leads to the fully turbulent boundary layer, with intense, fine-scale three-dimensional fluctuations.

The early nonlinear stage has been the subject of recent experimental, theoretical, and numerical work (Thomas 1983; Kachanov & Levchenko 1984; Saric, Kozlov & Levchenko 1984; Craik 1971; Herbert 1984, 1985; Wray & Hussaini 1980; Spalart 1984). Because the flow is still smooth, this stage is easier to study than the strongly nonlinear stage. It is also more important in terms of transition control, because full transition is inevitable once the strongly nonlinear stage has been reached. Thus, efforts to prevent transition (for instance pressure gradients, suction, or even active control of the waves) must be applied during the early stage, at the latest (Zang & Hussaini 1985*b*; Kleiser & Laurien 1985; Laurien & Kleiser 1985).

In most experimental studies a two-dimensional wave is introduced by means of a vibrating ribbon, so that it dominates the other unstable waves during the linear stage. This makes the experiment more reproducible. The theoretical and numerical studies, excepting Craik's (1971) work, also involve a dominant two-dimensional wave. This procedure should be considered as a first step toward the study of 'natural' transition. Natural transition generally involves wave packets, rather than single waves.

In the experiments of Klebanoff, Tidstrom & Sargent (1962) and Kovasznay, Komoda & Vasudeva (1962), with a vibrating ribbon, the first strong three-dimensional structures to appear were quasi-periodic in the streamwise direction, with the same period as the fundamental wave. The structures were also quasi-periodic in the spanwise direction, with a period of the same order. Spanwise material lines, often visualized by smoke, deform into Λ-shaped lines, suggesting the presence of 'Λ vortices' (however, since the flow contains distributed vorticity the concept of a 'vortex' is only loosely defined). As these structures evolve, and presumably under the effect of vortex stretching, the flow exhibits an increasing number of steep fluctuations or 'spikes' in the velocity field, which are the first signs of turbulence. This phenomenon was accurately simulated, numerically, by Wray & Hussaini (1980). Similar simulations were conducted in the channel by Orszag & Kells (1980).

The significant discovery of the last few years is that the streamwise period of the early three-dimensional structures can also be twice the period of the TS wave (Thomas 1983; Kachanov & Levchenko 1984; Saric *et al.* 1984). This is the 'subharmonic' type of breakdown, in which the Λ-structures are staggered as on a checkerboard. The experiments also indicate that subharmonic breakdown occurs for low and intermediate amplitudes of the TS wave, while the 'fundamental' or 'peak–valley' type occurs for higher amplitudes. If the wave amplitude is too low, it fails to cause transition and decays. Craik (1971) and Herbert (1984) have proposed small-disturbance theories that can predict an instability of the subharmonic type. Craik's model involves a resonant triad (a two-dimensional wave and two oblique waves), while Herbert's model involves the linear instability of three-dimensional waves in the presence of a finite-amplitude two-dimensional wave (secondary instability). Craik's mechanism is thought to dominate at low amplitudes (hence the designation C-type), while Herbert's mechanism describes intermediate-amplitude situations better (hence the designation H-type). Another version of Herbert's theory also predicts the fundamental or K-type breakdown (Herbert 1985).

The discovery of subharmonic breakdown presented a new challenge for numerical simulations. Preliminary results of the present study, presented by Spalart (1984), indicated that the two types of breakdown were indeed predicted, depending on the

amplitude (see also Zang & Hussaini 1985*a* and Laurien & Kleiser 1985). The quantitative agreement with experiments was fair. More complete and accurate results are presented here (a relatively minor programming error was corrected).

Experiments, small-disturbance theories, and numerical simulations all complement each other in the study of transition. Compared with small-disturbance models a direct numerical study, while more expensive, has several advantages. The simulation is fully nonlinear and the 'shape assumption' invoked by Herbert (1984) is not necessary. The spectrum is much larger, although it is still bounded and discrete. Random disturbances can be introduced and monitored concurrently in order to compare several possible instability mechanisms. Ensemble averages can be generated. The boundary-layer thickness and the amplitude of the primary disturbance evolve, as they do in the real flow, which has an impact on the secondary instability (a quasi-steady assumption is not made). Visualizations of the flow can be compared almost directly with experimental visualizations. The extension to more complex cases (pressure gradient, suction, crossflow, etc.) is straightforward. On the other hand, with the present method the mean flow is still treated as parallel and the fluctuations as spatially periodic, with transition occurring in time instead of space. Wray & Hussaini (1980) also used a parallel assumption and periodic conditions, mainly for reasons of computational cost. When the flow undergoes transition the range of length- and timescales widens rapidly, making an accurate numerical solution increasingly costly. The implications of these periodic assumptions will be discussed.

Besides the boundary conditions, the major choice to be made in a simulation of transition is the choice of the initial disturbances. In their numerical studies, Wray & Hussaini (1980, in the boundary layer) and Orszag & Kells (1980, in the channel) used a single pair of oblique waves as the initial three-dimensional disturbances. Their spanwise wavenumber was chosen to match experimental results. In the present study white noise was used as the three-dimensional disturbance in an effort to remove any bias. This required the use of a much larger period in the spanwise direction to provide a fine enough approximation of the continuous spectrum of the real flow. This large value of the period resulted in a fairly coarse numerical grid and prevented the extension of the simulations deep into the nonlinear stage. However, the present simulations can predict the dominant spanwise wavenumber instead of assuming its value, and the narrow- or broadband character of the instability. In some experiments there is evidence that the dominant spanwise wavenumber is dictated by persistent non-uniformities in the mean flow or in the two-dimensional wave (this was intentional in the work of Klebanoff *et al.*). However, in practical situations the disturbances (surface waviness, defects in the screens, free-stream noise, etc.) are more likely to have a random character.

2. Formulation

The approach is to solve the full, time-dependent, three-dimensional Navier–Stokes equations in the half-space over a plane wall. The initial condition is a Blasius boundary layer disturbed by a finite-amplitude, two-dimensional TS wave and low-amplitude, three-dimensional random noise. This corresponds to the conditions of an experiment in which the TS wave would be generated by a vibrating ribbon. It remains to choose proper boundary conditions; that is, to find a good compromise between the desire to conduct a thorough and unbiased simulation of the physics and the desire to obtain an accurate numerical solution at a reasonable cost.

In the experiments the disturbance introduced by the vibrating ribbon is periodic in time and quasi-periodic in the x-(streamwise) direction, in the sense that its amplitude and shape vary very little over one wavelength. In addition, at the early nonlinear stage, the experiments reveal spatial structures (Λ vortices) that are quasi-periodic both in the x- and in the z-(spanwise) direction. The wavelengths in the two directions are of the same order.

These observations suggest that periodic conditions in x and in z, with adequate values for the periods, should allow a valuable numerical simulation of the phenomena. Transition will occur in time instead of space, and only one or a few Λ-vortices will be contained in the numerical domain. Periodic conditions are mathematically convenient and allow a dramatic reduction in the size of the domain of integration, compared with a simulation that would represent the whole spatially developing boundary layer at once. On the other hand, they will result in a significantly different mean velocity profile unless a correction is made.

With periodic conditions in x, the mean flow is independent of x and parallel. The mean velocity component U is a function of the normal coordinate y and the time t, and satisfies

$$\frac{\partial U}{\partial t} - \frac{\partial \tau}{\partial y} = \nu \frac{\partial^2 U}{\partial y^2}. \tag{1}$$

The density is set to 1 and omitted, ν is the kinematic viscosity and τ is the Reynolds stress (τ is defined as $-\langle u'v' \rangle$, where u' and v' are the fluctuations with respect to the mean flow $U(y, t)$, $V = 0$ and $\langle\ \rangle$ denotes an average over the x- and z-directions). During the linear stage τ is negligible and (1) reduces to Stokes' first problem ($U_t = \nu U_{yy}$), for which the solution is a thickening error function. While this profile resembles the Blasius profile (both having zero curvature at the wall), its stability characteristics are quite different. The critical Reynolds number based on the displacement thickness δ^* and the free-stream velocity U_∞ is about 2000, instead of 520. This would make comparisons with experiments impossible, as illustrated in the next chapter. This is why it was decided to add a small correction to the Navier–Stokes equations so that the laminar solution has a Blasius profile.

In addition, in the spatially developing boundary layer the TS-wave amplitude and the boundary-layer thickness grow simultaneously, on the same long 'viscous' lengthscale $U_\infty \delta^{*2}/\nu$. A given wave becomes unstable and starts growing when the flow crosses 'Branch I' on the stability diagram (Schlichting 1979). It becomes stable again and starts decaying when the flow crosses 'Branch II'. If the mean flow did not evolve, the wave would experience sustained exponential growth or decay. This difference is important, and it was decided that the modified form of (1) should allow the thickness to grow in time, while retaining a Blasius profile. The procedure is the following.

The solution of the Blasius equation provides the boundary-layer profile $U_B(y, X)$ as a function of y and of X, the distance from the leading edge. A linear correspondence between time t and distance X is made:

$$X = X_0 + ct. \tag{2}$$

The celerity c is chosen to match the growth rate of the boundary-layer thickness and the growth rate of the TS wave. The group velocity c_g is known to relate the temporal growth rate of spatially periodic TS waves and the spatial growth rate of time-periodic waves, if the growth rates are small and the mean flow is treated as parallel (Gaster 1962). Thus, c should be taken equal to c_g. The group velocity is not

quite constant, because the boundary layer thickens, but this effect is weak. In the range of Reynolds numbers considered here, the group velocity is between about $0.38U_\infty$ and $0.42U_\infty$. A constant value $c = 0.4U_\infty$ will be used.

Introducing (2) into the function $U_B(y, X)$ defines the 'desired' mean velocity profile $U_B(y, t)$. The correction consists in adding the quantity $\partial U_B/\partial t - \nu\partial^2 U_B/\partial y^2$ to the U-component momentum equation. It depends only on y and t. Equation (1) becomes

$$\frac{\partial U}{\partial t} - \frac{\partial \tau}{\partial y} = \nu\frac{\partial^2 U}{\partial y^2} + \frac{\partial U_B}{\partial t} - \nu\frac{\partial^2 U_B}{\partial y^2}. \tag{3}$$

If, in addition, the initial profile is

$$U(y, 0) = U_B(y, 0), \tag{4}$$

the solution $U(y, t)$ of (3), (4) will satisfy

$$U(y, t) = U_B(y, t) \tag{5}$$

as long as τ is negligible. This applies to the laminar flow, and to the transitioning flow until the disturbances reach a nonlinear level.

This procedure of solving the mean momentum equation, albeit with an artificial term added, is preferable to the cruder procedure of just imposing (5) for all times, because it allows the disturbances to deform the mean-velocity profile and extract energy from it. The beginning of the nonlinear stage is clearly indicated. In practice, one can monitor the shape factor H of the mean profile (H is defined as δ^*/θ where δ^* is the displacement thickness and θ the momentum thickness). The correction term acts only on the mean flow, and has no direct effect on the fluctuations. Of course, when the velocity profile loses its Blasius shape, the correction becomes inadequate. However, breakdown occurs on the fast, convective timescale δ^*/U_∞ and the correction term, which acts on the slow, viscous timescale δ^{*2}/ν, has little effect. This fact was recognized by Wray & Hussaini (1980). They did not apply any correction but started their simulation shortly before breakdown, so that the mean profile remained close to the initial Blasius profile until breakdown occurred (the displacement thickness increased only by about 20%). In the present study the boundary layer is followed for a much longer time (so that the dynamics can select the most unstable three-dimensional disturbances), hence the need for a correction. The displacement thickness roughly doubles during the simulation.

The numerical method designed by Spalart (1986) for the solution of the three-dimensional time-dependent Navier–Stokes equations in a half-space is used. This method is spectral in space, with infinite-order accuracy, and uses second-order-accurate finite differences in time. The correction term is easily handled by the Runge–Kutta time-integration scheme. The initial TS-wave amplitude is varied to obtain different types of breakdown. The overall amplitude of the random disturbances is also varied, as is the sequence of computer-generated random numbers. The amplitude of the three-dimensional random disturbances is statistically the same for all wave vectors in the (x, z)-plane (white noise). The disturbances also extend all across the domain in the y-direction; several types of random y-dependence were tried without causing significant differences in the results. Thus the (arbitrary) disturbances are as unbiased as possible. Introducing selected three-dimensional disturbances is of course possible, but the resulting proliferation of additional parameters with unknown practical significance was thought to be undesirable.

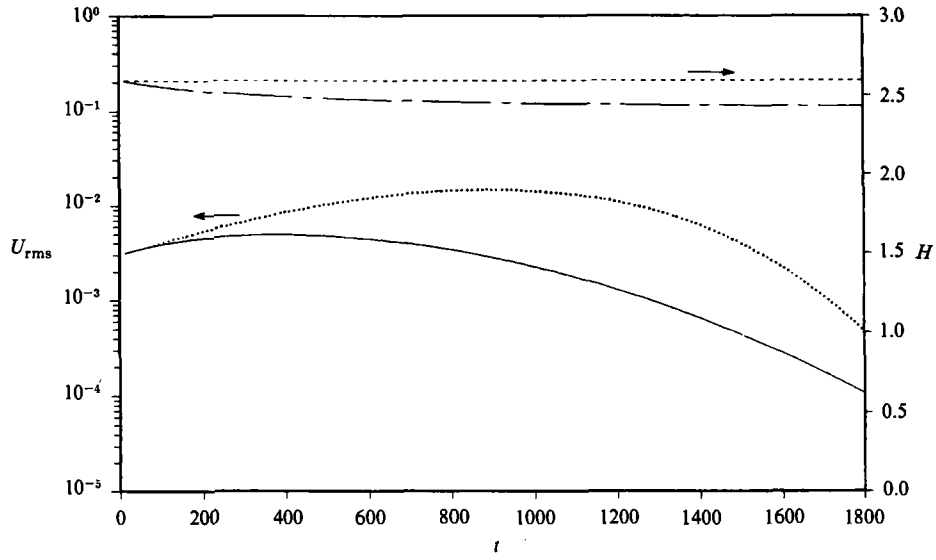

FIGURE 1. Comparison of simulations with and without forcing: ---, shape factor H; ···, TS-wave amplitude. Without forcing: -·-, shape factor; ——, TS-wave amplitude.

3. Results

3.1. *Physical and numerical parameters*

The spatial and temporal accuracy of the method, when applied to a single TS wave, was tested by Spalart (1986). These tests showed very good accuracy with the resolution that will be used throughout, namely 27 Jacobi polynomials and a value of about $3\delta^*/U_\infty$ for the time step. The amplitude ratio of the wave, from Branch I to Branch II, is also of interest and depends directly on the value of c. With $c = 0.4U_\infty$ the ratio is about 17 for the TS wave that will be considered in this study, which is the right magnitude. In the experiments of Saric *et al.* (1984) the ratio was about 25, and part of the growth was an artifact due to the smoke wire disturbing the mean flow.

Figure 1 shows the effect of forcing the mean-velocity profile (see (3)). It would of course be preferable not to have to add such a term and justify the value of c. Two simulations were conducted with the same initial condition: a Blasius mean profile and a two-dimensional TS wave, part-way between Branch I and Branch II. The duration of the simulations was typical, extending beyond Branch II. The forced simulation displays a constant shape factor; the wave grows until a time of about 900 and then decays. In contrast, in the unforced simulation the shape factor reaches about 2.4, the error-function value, in about 700 time units. More importantly, the wave starts decaying at time about 400 and its amplitude is much lower than in the forced simulation. This test shows that unless the simulation is started shortly before breakdown, in which case the flow will not have time to lose memory of the shape of the initial three-dimensional disturbances, forcing is necessary to maintain even a reasonable correspondence with the spatially developing flow.

The three-dimensional results will now be described. The conditions of Saric *et al.*'s (1984) experiment were reproduced as closely as possible. In a spatially developing boundary layer the frequency f of the TS wave is independent of X. In a time-

developing boundary layer it is the streamwise wavenumber α that is independent of t. The non-dimensional frequency F and the non-dimensional wavenumber a, defined by

$$F \equiv 10^6 \frac{2\pi f \nu}{U_\infty^2}, \quad a \equiv 10^3 \frac{\alpha \nu}{U_\infty}, \tag{6}$$

are related by

$$F = 10^3 \frac{c_\phi}{U_\infty} a, \tag{7}$$

where c_ϕ is the phase velocity of the wave. The quantity c_ϕ / U_∞ varies slightly in the neighbourhood of 0.36 as the thickness grows, so that F varies by a few percent in the simulation. With the wavenumber a set to 0.21, F is close to 76, the value chosen by Saric *et al.* (1984). The Reynolds number $R \equiv (U_\infty X/\nu)^{\frac{1}{2}}$ at Branch II, for $a = 0.21$, is about 920.

When periodic conditions are imposed in a numerical simulation the values of the periods Λ_x and Λ_z, in the x- and z-directions, are to some extent arbitrary. Larger values are preferable, but increase the computational cost. The period Λ_x must be a multiple of the period Λ_{TS} of the TS wave to accommodate it; subharmonic waves are also expected. This motivates the choice $\Lambda_x = 2\Lambda_{TS}$. Thus the lowest streamwise wavenumber in the simulation is $a = 0.105$. The period is about 40 times the displacement thickness at Branch II. There are 16 points in real space, and 5 non-zero wavenumbers. In the z-direction the lowest wavenumber is $b = 0.035$; the numerical period is about 120 displacement thicknesses. This large period is chosen to allow a fine description of the spectrum in the z-direction. In most cases, there are several z-wavenumbers within the bulge in the spectrum. Depending on the cases, there are 48 or 96 points in the z-direction. The two-dimensional spectra that will be presented show how, in high-amplitude cases, higher spanwise wavenumbers develop significant energy. This is why 96 points are used for these cases, while 48 are sufficient at low amplitudes. The same plots show that the resolution in the x-direction is sufficiently fine.

With these values, the Reynolds number based on the free-stream velocity and the grid spacing in the x- or z-direction is several thousand; the grid can be quite coarse because the viscosity plays a very weak role in these directions. This is acceptable as long as the flow is smooth, but when breakdown occurs the spectrum 'fills up' very rapidly and the simulation is no longer reliable. Simulations deeper into the breakdown phase will be possible only with much finer resolution and presumably with a smaller domain (Wray & Hussaini 1980).

The most important parameter is the maximum root-mean-square (r.m.s.) amplitude A_{max} of the TS wave. This maximum is taken versus both y and X (or R). In the X-direction this peak corresponds to Branch II, unless nonlinear effects are present. If A_{max} is below about 0.4 %, three-dimensional breakdown does not occur while the TS wave is the dominant disturbance (breakdown occurs much later, with a different mechanism). Between 0.4 % and about 3 %, subharmonic C- or H-type breakdown occurs, with increasing spanwise wavenumber. Above 3 % a mixed-type breakdown is observed; a clear-cut K-type breakdown is never observed. In the experiments, the threshold amplitudes were lower: about 0.25 % for subharmonic breakdown, and 1 % for K-type. These discrepancies have already been observed by Spalart (1984) and will be discussed further.

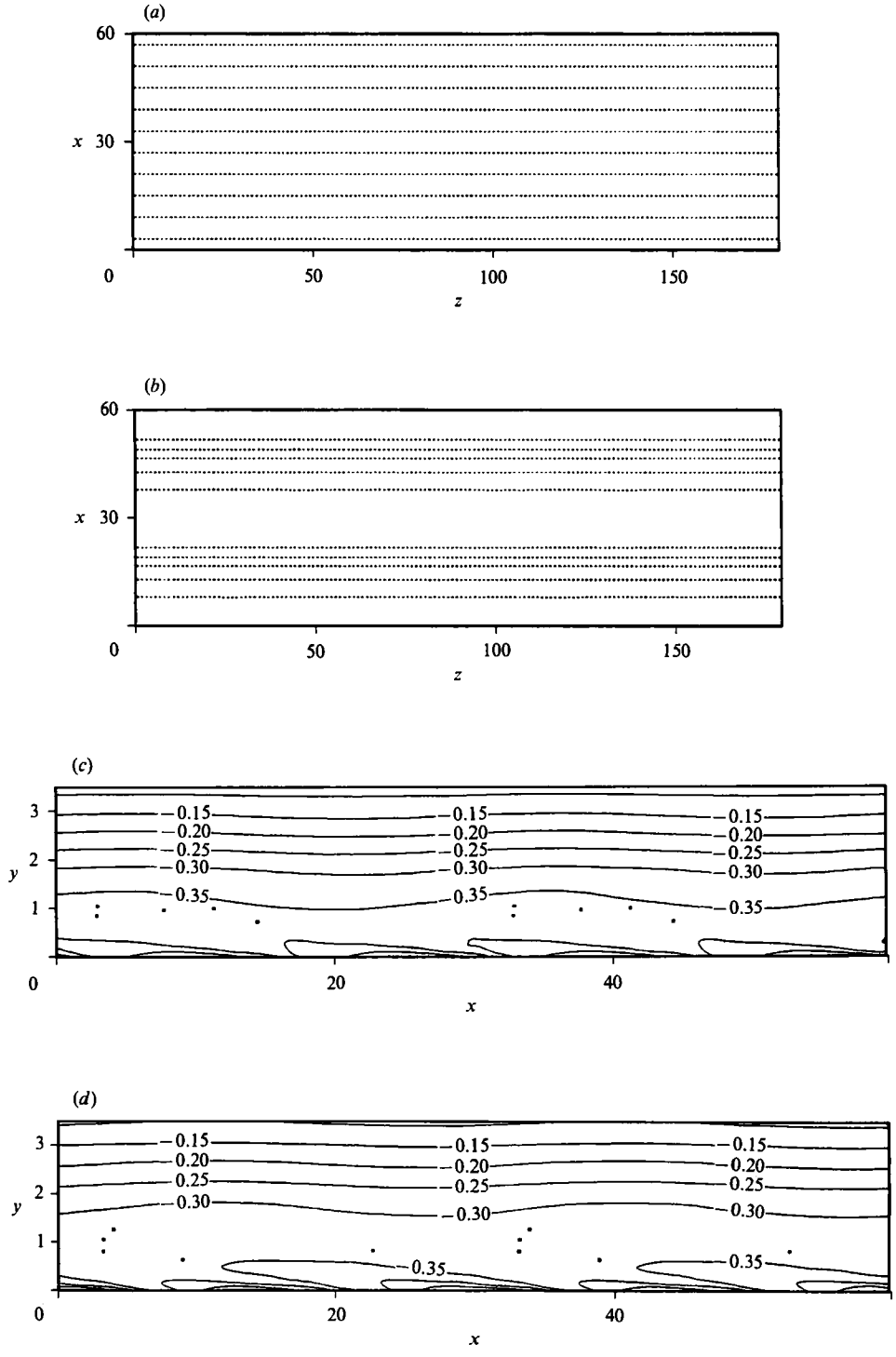

FIGURE 2(*a–d*). For caption see facing page.

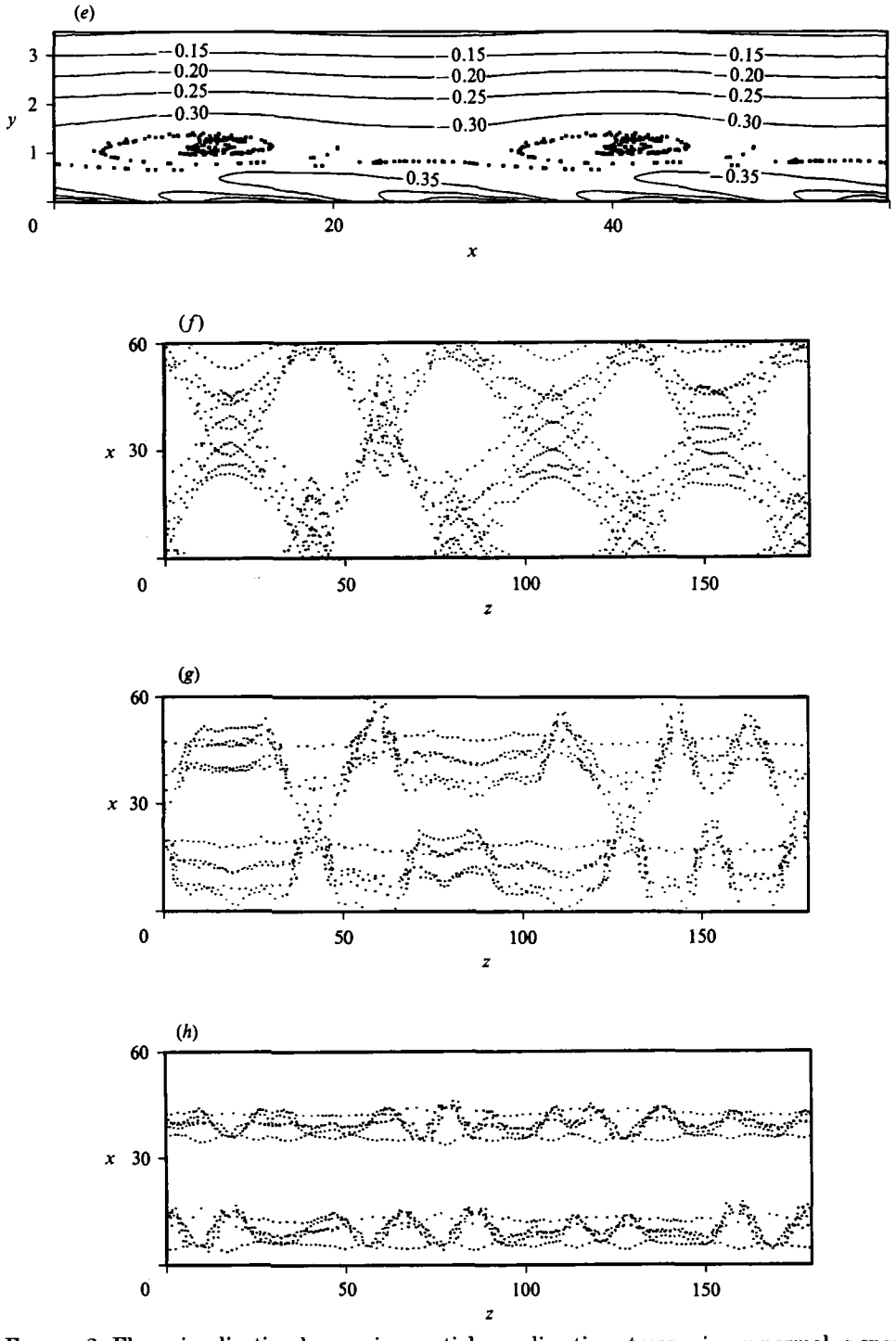

FIGURE 2. Flow visualization by passive particles. x-direction streamwise, y normal, z spanwise; ——, vorticity contours. (*a*) Initial position; (*b*), (*c*), (*d*) at different times before three-dimensional breakdown; (*e*) before breakdown, with large number of particles; (*f*) beginning of breakdown, $A_{\max} = 1\,\%$; (*g*) beginning of breakdown, $A_{\max} = 1.5\,\%$; (*h*) beginning of breakdown, $A_{\max} = 4.8\,\%$.

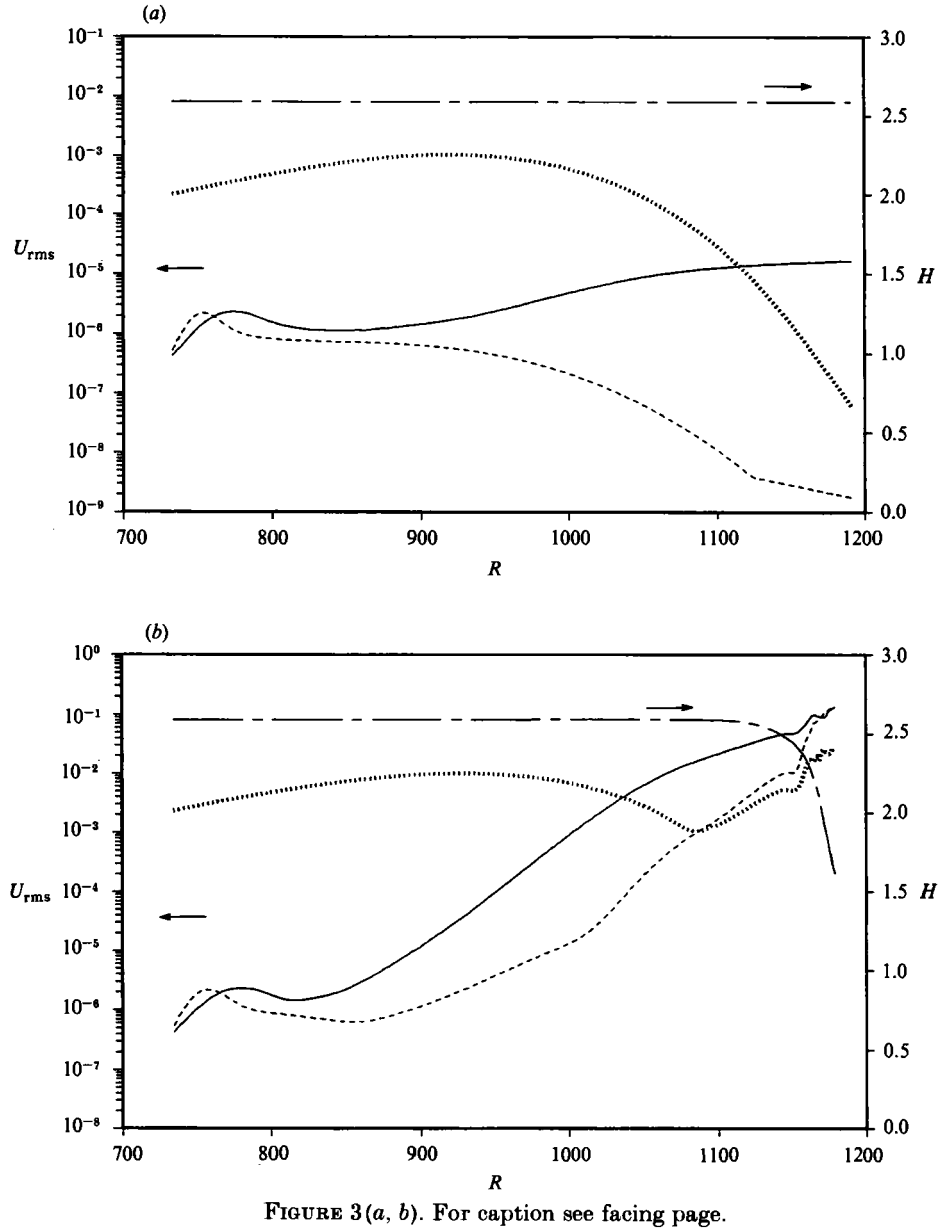

FIGURE 3(*a*, *b*). For caption see facing page.

3.2. *Visualizations*

Visualizations of the flow using passive particles will be shown first, and can be compared with the experimental visualizations using smoke (Saric *et al.* 1984). The motion of the particles is computed using linear interpolation in space and the Runge–Kutta third-order scheme in time (see Spalart 1986). Figure 2(*a*) shows the initial position of the particles. The coordinates are non-dimensionalized by U_∞ and $10^3\nu$. The non-dimensional displacement thickness is between 1.25 and 2. Six spanwise lines of 144 particles each are released at regular intervals in x. The height of release

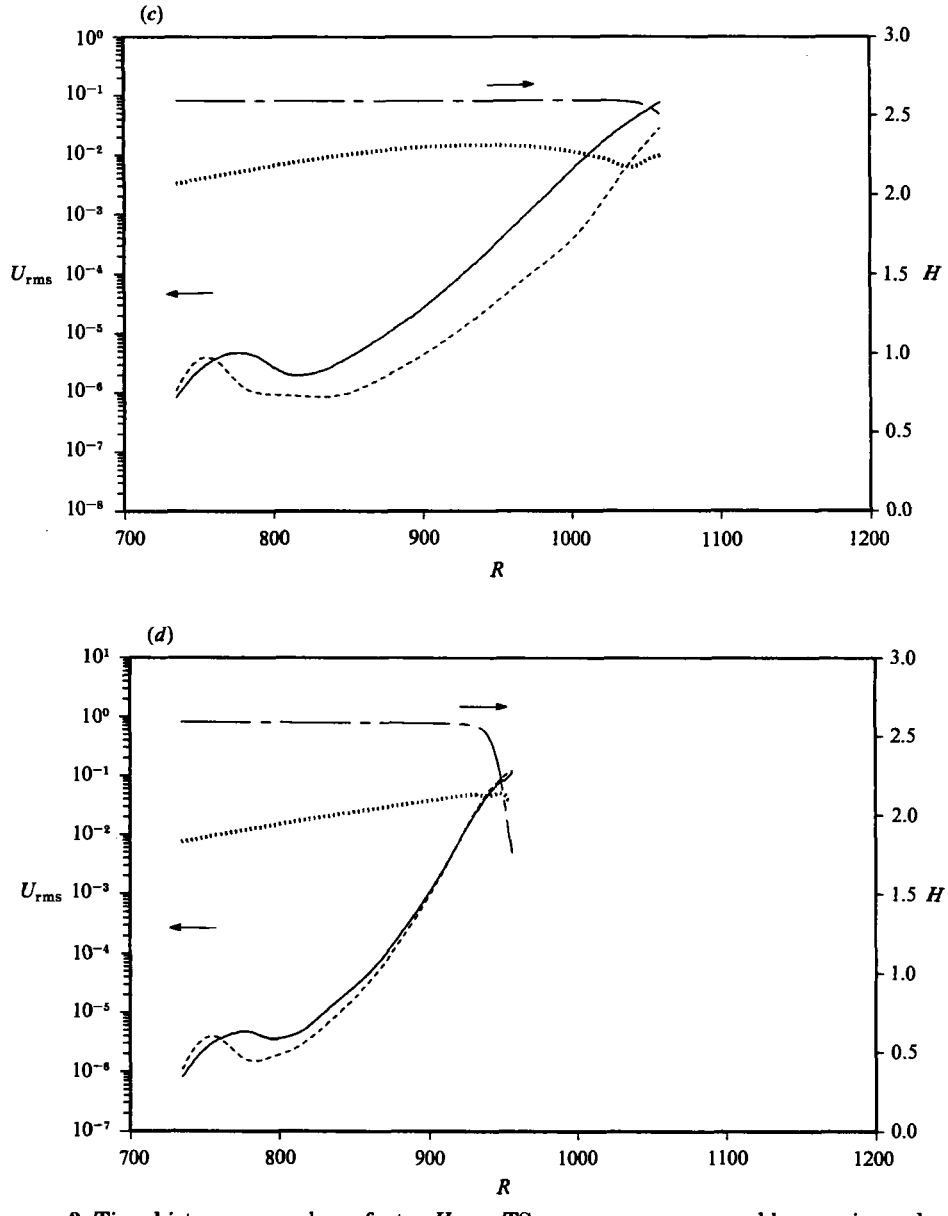

FIGURE 3. Time history, ——, shape factor H; ···, TS-wave r.m.s.; ——, subharmonic-mode r.m.s.; – – –, fundamental-mode r.m.s. (*a*) $A_{\max} = 0.1\%$; (*b*) $A_{\max} = 1\%$; (*c*) $A_{\max} = 1.5\%$; (*d*) $A_{\max} = 4.8\%$.

is adjusted so that the particles are near the critical layer when breakdown occurs. This is important: by keeping the particles in phase with the flow structures one greatly enhances the correspondence between the particle-line pattern and these flow structures. The particles cannot be *exactly* in the critical layer, if only because this layer moves up as the boundary layer thickens.

Figure 2(*b*) shows the particles after some time, but before three-dimensional effects are felt. The particles clustered into two bundles, revealing the two TS waves

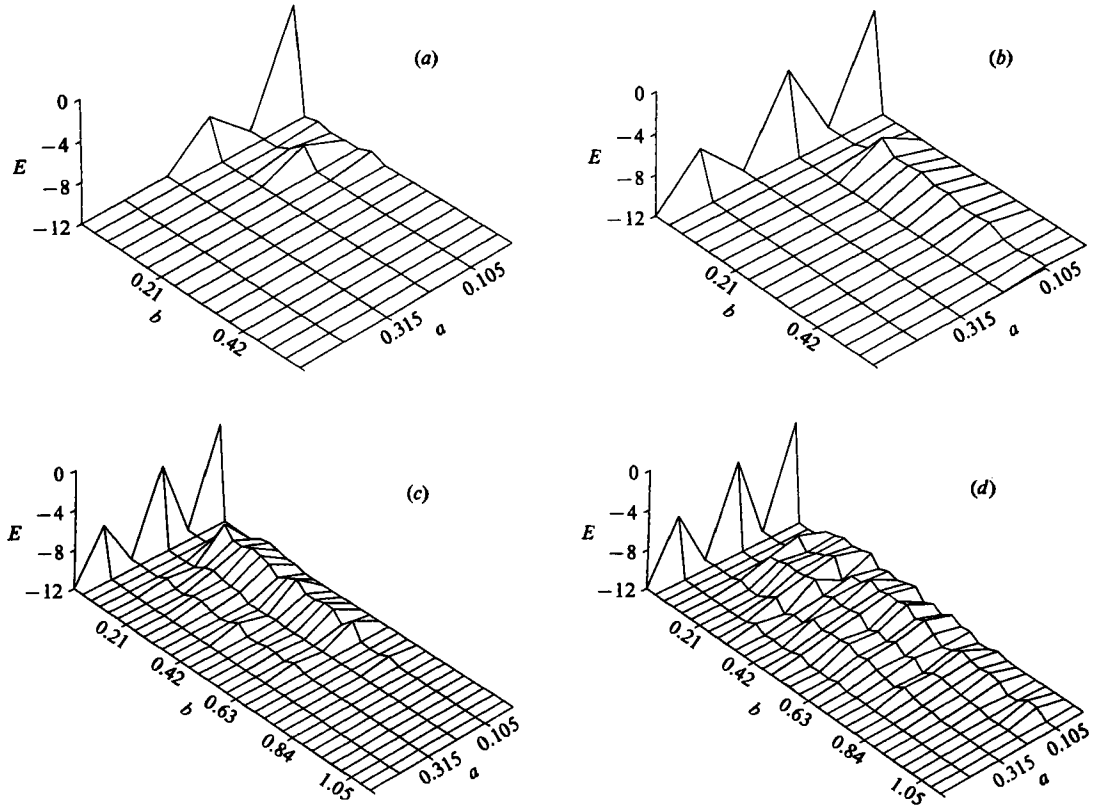

FIGURE 4. Two-dimensional energy spectra before breakdown; a streamwise wavenumber, b spanwise; energy scale logarithmic, base 10. (a) $A_{\max} = 0.1\%$, $R = 1108$; (b) $A_{\max} = 1\%$, $R = 913$; (c) $A_{\max} = 1.5\%$, $R = 912$; (d) $A_{\max} = 4.8\%$, $R = 855$.

contained in the domain. Since the observation of these bundles as they subsequently deform is a major tool in both experimental and numerical studies, it is important to know which part of the wave is marked by the bundles. In particular, do they follow a 'vortex'? Figures 2 (c, d) are plots in an (x, y)-plane in the same situation as figure 2(b) (under the effect of the two-dimensional wave, but before breakdown) and at two different times. The y-direction is magnified. The positions of the particles and vorticity contour are superimposed. Figures 2 (b, c, d) are typical of the behaviour at other times. The particles tend to gather in regions of higher-than-average vorticity, which are indicated by the upward bending of the vorticity contours.

This gathering is statistical rather than systematic. If a large number of particles is released, they form a 'cloud' which is densest in the high-vorticity region (see figure 2e). Figure 2(e) corresponds most closely to the experimental situation, in which smoke is continuously emitted by the smoke wire and forms one cloud per TS-wave period. In a reference frame moving with the phase velocity of the wave, the trajectories in the vicinity of the critical layer are shallow orbits. As a result, the particles that are caught in these orbits form a cloud that follows the wave. What figure 2(e) shows is that the centre of the orbits roughly coincides with the 'vortex' carried by the TS wave, which was not obvious *a priori*.

Figure 2(f) shows the particles at the time of breakdown, with $A_{\max} = 1\%$, revealing a staggered pattern. The spanwise wavenumber b is 0.14, in very good

agreement with the value of Saric *et al.* (1984). Figure 2(*g*) is at $A_{\max} = 1.5\%$; the pattern is still staggered but is less regular, and the structures are narrower; b is about 0.2. This value agrees with the value measured by Saric *et al.* for an H-type breakdown, but their value of $A_{\max}$ was different (0.4%). The appearance of figures 2(*f*, *g*) is very similar to the experimental visualizations. Figure 2(*h*) is at $A_{\max} = 4.8\%$; the breakdown pattern is irregular, with the Λ-structures staggered in some regions and aligned in others. A breakdown pattern with the Λ-structures all aligned was never observed for any wave amplitude and time of visualization. This will be discussed further.

3.3. *Quantitative results*

Figure 3 shows histories of the shape factor H of the boundary layer, the amplitude of the TS wave, and the r.m.s. of the three-dimensional fundamental components (oblique waves with the same streamwise wavenumber as the TS wave) and subharmonic components (wavenumber half that of the TS wave). The r.m.s. is defined with respect to the average over an (x, z)-plane; the maximum of this quantity versus y is then taken, and is plotted versus R. The shape factor is plotted to signal when the mean-velocity profile starts to depart from the Blasius shape. When breakdown occurs, H shows a clear tendency to decrease from its laminar value of 2.6 toward the turbulent value, about 1.5.

In figure 3(*a*), $A_{\max} = 0.1\%$. This amplitude is too low for breakdown to occur while the TS wave is the primary disturbance. There is a period of growth of the subharmonic mode. A referee to this paper pointed out that this growth could reflect the primary instability of the subharmonic mode, and not be related to the two-dimensional wave; this point will be discussed below. The TS wave decays beyond Branch II, following linear theory. The fundamental-mode energy also decays steadily. In figure 3(*b*), with $A_{\max} = 1\%$, the subharmonic component becomes unstable, grows rapidly, and causes breakdown. A similar behaviour is observed in figure 3(*c*), with $A_{\max} = 1.5\%$. In both cases, a sudden reversal of the decay of the TS wave is the first indication of nonlinearity. This was also observed by Kachanov & Levchenko (1984). The TS wave is presumably receiving energy from the subharmonic components throughout the nonlinear term (the subharmonic amplitude has reached several percent). Finally, in figure 3(*d*) with $A_{\max} = 4.8\%$, the fundamental-mode energy becomes significant. However, it does not dominate the subharmonic energy. In this last case, the occurrence of breakdown is revealed by the shape factor and the TS-wave amplitude simultaneously.

Figure 4 presents a more detailed description of the fluctuations, using two-dimensional spectra. The u component in an (x, z)-plane was Fourier transformed in the x- and z-directions and the energies of the four wavevectors $(\pm a, \pm b)$ were added. The plane chosen is near the critical layer; the fluctuations are known to be quite strong in that layer. A logarithmic scale is used for the energy, and values lower than 10^{-12} are not plotted to distinguish between the random noise and the relevant, energetic wave vectors. Except for the mean flow and the TS wave, any component that exceeds 10^{-12} in energy has experienced a significant amplification since the beginning of the simulation. In the far corner of the figure is the mean component. Along the far-left boundary are the two-dimensional components (the TS wave and its higher harmonic).

In figure 4(*a*) with $A_{\max} = 0.1\%$ a three-dimensional wave, while not strong enough to cause breakdown, has been amplified and is clearly defined. The spectrum shows a sharp peak with spanwise wavenumber $b = 0.14$ which suggests that the

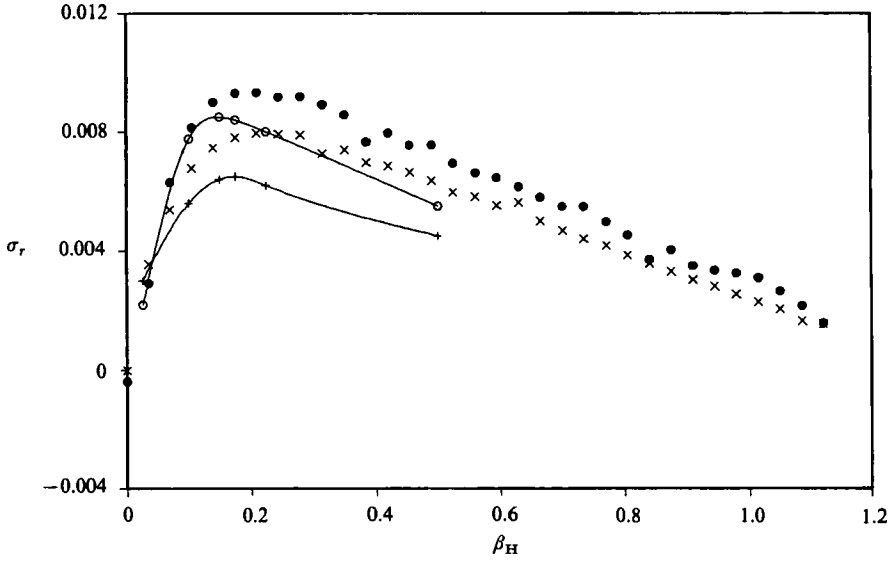

FIGURE 5. Growth-rate of three-dimensional disturbances. Present results: ●, subharmonic; ×, fundamental. Herbert (1985): ○, subharmonic; +, fundamental.

growth cannot be due to primary instability, for the primary instability is not very selective in terms of spanwise wavenumber (the unstable region is kidney-shaped and centred on the $b = 0$ axis). In figure 4(*b*) with $A_{max} = 1\%$ the subharmonic component dominates, with a sharp peak at $b = 0.14$ (as indicated by the visualizations) and a swelling at higher values ($b \approx 0.25$). At a higher amplitude, 1.5%, the spectrum is much broader (figure 4*c*). There is still a peak at $b = 0.14$, but there is also a broad band of energetic wavenumbers from $b \approx 0.1$ to $b \approx 0.7$. These results are in agreement with Herbert (1984). At the highest amplitude, $A_{max} = 4.8\%$, both the subharmonic and the fundamental mode have acquired energy and have a broad spectrum (figure 4*d*), which results in the disordered pattern of figure 2(*h*). Again the results agree with Herbert's (1985) results, in that the subharmonic mode is still strong even at high TS-wave amplitudes.

To make a quantitative comparison between Herbert's results and those obtained here, the growth rates computed by Herbert (1985) at $F = 58.8$ and $A = 1.4\%$ were computed with the present method. The boundary-layer thickness and the TS-wave amplitude were artificially kept constant to simulate Herbert's conditions (quasi-steady assumption). The flow was allowed to evolve until the growth rates of the three-dimensional disturbances became steady, indicating that the most unstable components had been selected. The comparison is shown in figure 5, using Herbert's units, and is satisfactory.

The determination of the dominant spanwise wavenumber allows one to test Craik's hypothesis (Craik 1971). For Craik's mechanism to explain the growth of the oblique waves, their phase velocity and that of the two-dimensional wave must be close. In figure 6(*a*) the band of energetic spanwise wavenumbers is plotted as a function of A_{max}. The wavenumbers were deduced from the visualizations; they increase with A_{max}. In figure 6(*b*) the phase velocity (in the x-direction) of the two-dimensional and of the dominant oblique waves are plotted. When A_{max} exceeds about 1%, most of the energy is carried by wavenumbers that do not satisfy Craik's

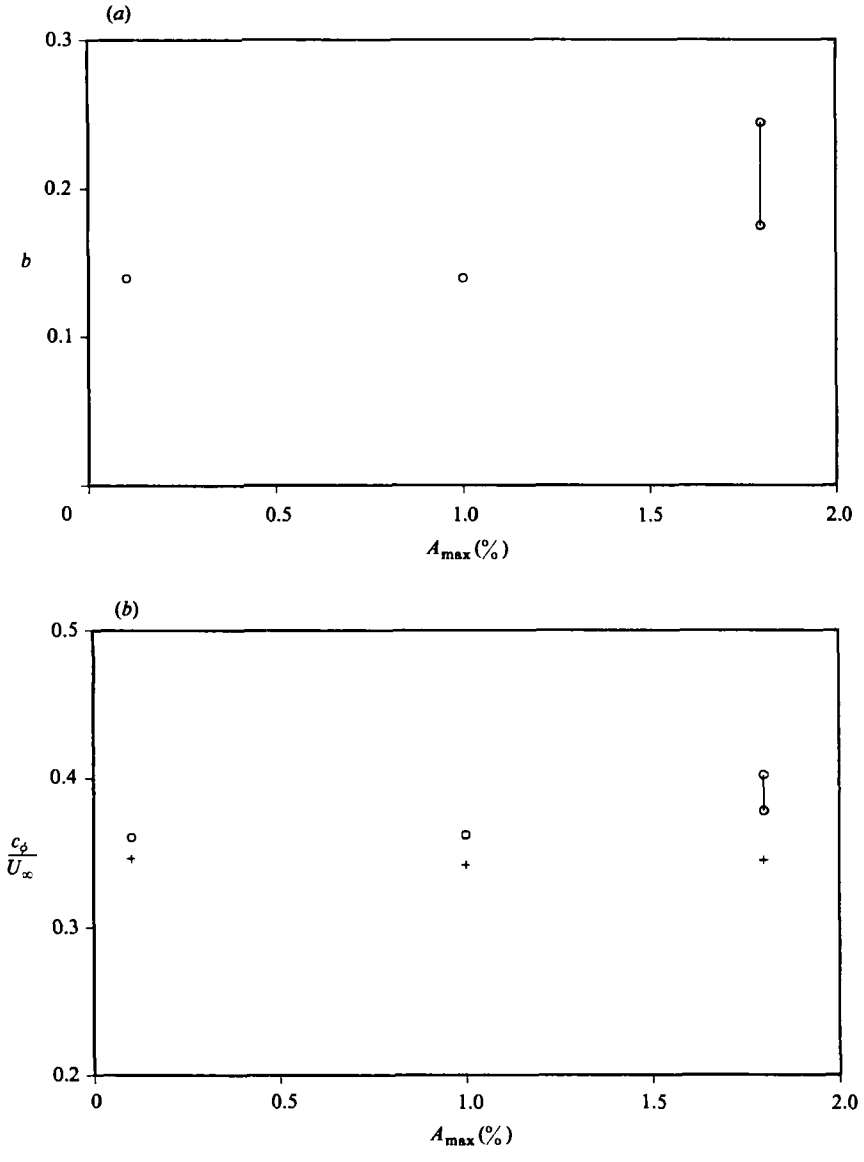

FIGURE 6. Characteristics of dominant subharmonic waves. (*a*) Spanwise wavenumber; (*b*) phase velocity. ○, three-dimensional waves; +, TS wave.

criterion. These results support Herbert's (1984) contention that Craik's mechanism is active at low TS-wave amplitudes, but cannot account for all of the three-dimensional activity at high amplitudes. Herbert's model describes ribbon-induced transition better; Craik's may be more relevant in natural transition.

3.4. *Sensitivity to some of the parameters*

The disturbance created by a vibrating ribbon in an experimental boundary layer is not a pure TS wave, and it takes some distance for the other components to decay. In addition the ribbon and the smoke-wire disturb the mean-velocity profile (Saric *et al.* 1984). This is why they must be far enough upstream of the region where

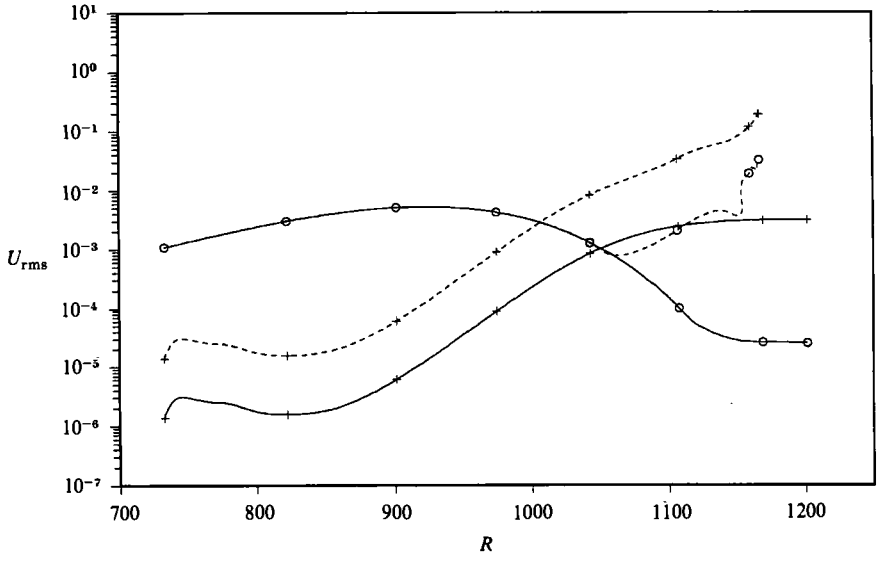

FIGURE 7. Effect of noise level, $A_{\max} = 0.5\%$. ○, TS wave; +, three-dimensional waves. ——, low level; – – –, high level.

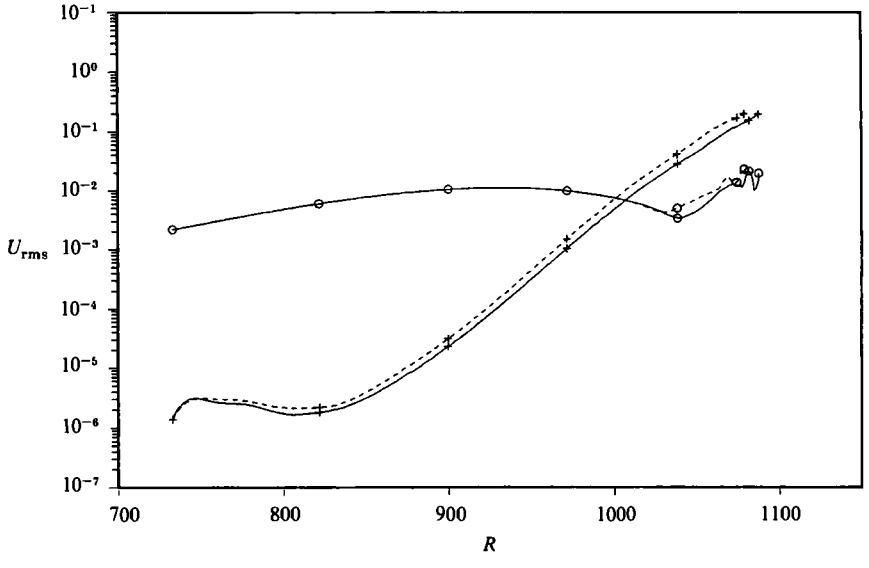

FIGURE 8. Effect of random-number sequence, $A_{\max} = 1.5\%$. ○, TS wave; +, three-dimensional waves. ——, first sequence; – – –, second sequence.

measurements are taken. This distance is the 'fetch'. In the simulations a pure TS wave can be input, and the mean profile is not disturbed at all. Thus the need for a long fetch is not as strong. However, the three-dimensional disturbances are random, and no attempt is made to control their shape. Thus there is a period during which the various components get sorted so that only the unstable, or weakly stable, ones survive. This is revealed by figure 3: the shape factor remains at 2.6 and the amplitude of the TS wave grows smoothly from the initial station, but the

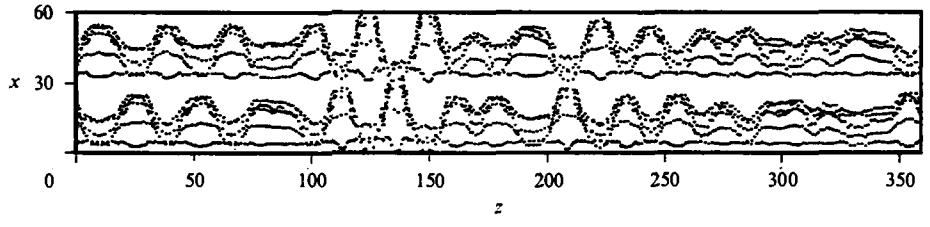

FIGURE 9. Simulation with increased A_z, $A_{\max} = 1.5\%$. See figure 2(*g*).

three-dimensional energy has rapid variations at the very beginning of the simulation. However, figure 3 also shows that this 'unphysical' regime is over long before breakdown occurs. This means that the fetch is long enough. The smoothness of the spectra, presented in figure 4, confirms this impression. Simulations were conducted with longer fetches (starting near Branch I) and the results were not significantly different.

The type of the breakdown mostly depends on the peak amplitude $A_{\max}$ of the TS wave. However, it also depends on the initial amplitude A_{3D} of the three-dimensional random disturbances, or 'noise level', especially if $A_{\max}$ is near a threshold. Simulations were conducted with $A_{\max} = 0.5\%$ and two values of A_{3D}. The r.m.s. of the three-dimensional components, after the initial transient, was about 2×10^{-5} and 2×10^{-6}, respectively. The results are shown in figure 7. Breakdown occurs only with the higher value of A_{3D}. This illustrates the impossibility of sharply defining threshold values in terms of $A_{\max}$ alone. The difference between the experimental and the numerical estimates of the lowest value of $A_{\max}$ that will result in breakdown (0.25% and 0.4%, respectively) is not serious.

The effect of the random numbers used for the initial disturbance was also studied. Figure 8 shows the energy histories for two simulations which had the same disturbance amplitude but different random-number sequences. The three-dimensional energy is at slightly different levels, but the growth pattern is the same. Because of the different level of energy, breakdown occurs at slightly different stations. The scatter in the breakdown Reynolds number is of the order of 10, and is quite small compared with the scale of the early stages of transition, which is hundreds of Reynolds-number units. This result suggests that the use of random numbers for the initial disturbance is appropriate.

Finally, the effect of the computational periods Λ_x and Λ_z which, ideally, would be infinite, was studied by doubling them. Figure 9 is a visualization of the flow with Λ_z doubled and $A_{\max} = 1.5\%$. The breakdown pattern is still somewhat irregular, but is obviously an H-type. There are no major differences between this figure and figure 2(*g*). This indicates that the original value of Λ_z is sufficient. The period Λ_x was then doubled, to investigate the possibility of another period-doubling in the x-direction, similar to the difference between K- and H-type breakdown. Figure 10(*a*) is a visualization of the flow. The difference between the two halves of the domain, in the x-direction, is small but noticeable. This suggests that enough randomness was present to trigger an instability, if such an instability exists. The spectrum, shown in figure 10(*b*), reveals significant energy in the 'sub-subharmonic' region. However, the first subharmonic mode still dominates. The results in figures 9 and 10 suggest the possibility of generating incipient turbulent spots by using large enough periods both in the x- and z-directions.

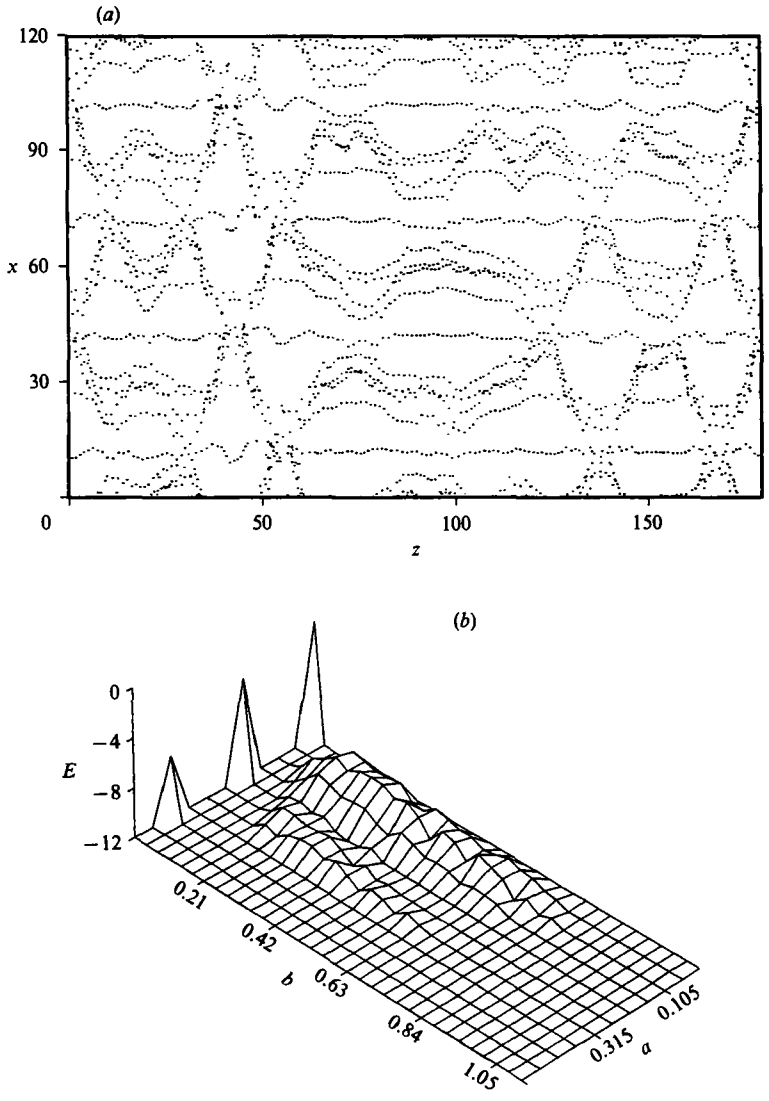

FIGURE 10. Simulation with increased A_x, $A_{\max} = 1.5\%$. (*a*) Passive particles, (*b*) spectrum. See figures 2(*g*) and 4(*c*).

3.5. *Discussion*

The results presented in this section are in good agreement with Herbert's analysis, and their sensitivity to the arbitrary parameters that had to be prescribed was shown to be very moderate. The agreement with Saric *et al.*'s (1984) experimental results is good for the lower values of $A_{\max}$. On the other hand, the computed threshold between the C-type breakdown (wide structures in the z-direction) and the H-type (narrower structures) is over 1%, when the experimental value is about 0.35%. In addition, a pure K-type breakdown is never predicted even at high amplitudes. The trend is for the numerical results to match the experimental results at lower amplitudes. In terms of the breakdown location, both sets of results show C-type breakdown occurring beyond Branch II, H-type breakdown near Branch II, and K-

or mixed-type breakdown upstream of Branch II, the computed breakdown being slightly farther downstream (compare our figure 3 and Saric *et al.*'s figure 5). The agreement could probably be improved further by raising the noise level in the simulations.

The behaviour of the flow for $A_{\max}$ near the C- to H-type threshold is illustrated by the spectra in figure 4(*a–c*). They show that the C-mode ($b = 0.14$) grows first, when the TS-wave amplitude is low. Further downstream, if $A_{\max}$ is high enough, the H-mode (broadband) grows. It may or may not 'catch up' with the C-mode before breakdown. Figures 2(*f*) and 4(*b*) show that with $A_{\max} = 1\,\%$ it did not catch up, resulting in a C-type breakdown. The competition between the two modes depends, to some extent, on the fetch and on the noise level. The same can be said of the competition between the H- and K-modes; figure 3(*d*) shows the K-mode starting from a lower level, but consistently having a slightly larger growth rate than the H-mode. To study these fine effects one could consider 'shaping' the spectrum of the random disturbances instead of keeping it white, but this would enlarge the parameter space to be explored. One could also input random disturbances continuously instead of only initially; this would shorten the 'memory' of the flow by preventing the decay of some waves to very low levels of energy, and may be closer to the experimental situation. It could essentially eliminate the influence of the fetch.

One should note that in the experimental pictures, the breakdown that is interpreted as a K-type looks much more irregular than the C- and H-type breakdowns and has some features of a mixed-type breakdown (Thomas 1983; Saric *et al.* 1984). Herbert (1985) studied Klebanoff *et al.*'s (1962) experiment in detail. The experiment produced a K-type breakdown, but Herbert's theory predicts an H-type in the sense that the computed subharmonic-mode growth rates are consistently higher than the fundamental-mode growth rates (figure 5). He concluded that in the experiment the fundamental mode was receiving more energy than the subharmonic mode because of non-uniformities of the mean flow in the z-direction. These non-uniformities may be 'chopped' by the ribbon at the frequency of the TS wave. Recall also that the K-type instability mechanism is not very selective in terms of spanwise lengthscales. One may ask whether, by adding strips of tape to the plate, Klebanoff *et al.* (1962) merely suppressed the wavering of a well-defined K-type pattern, or actually changed the breakdown type from mixed (as in figure 2*h*) to K. The present results, and Herbert's, may prompt a more cautious interpretation of the experimental visualizations.

These considerations show that the disagreement between numerical and experimental results cannot be considered as final unless *all* the disturbances, including the ones that are classified as 'noise', are completed controlled. One should also keep in mind the sources of error in the theoretical and numerical studies. The ideal situation is a perfectly uniform (in z and t), spatially developing boundary layer, with spatially developing disturbances. Like Herbert, we are treating a parallel mean flow and time-developing disturbances. The non-parallel character of the mean flow is known to affect the critical Reynolds number of TS waves to some extent; its effect here is unknown. The periodic assumption loses some of its validity precisely at the beginning of the nonlinear stage, when the growth rates increase (the experimental visualizations show the three-dimensionality changing from unnoticeable to strong in about three wave lengths). Thus the question of which type dominates in the ideal situation can receive a definitive answer only from refined experiments, or from simulations or theories in which the parallel-mean-flow and periodicity assumptions have been discarded.

4. Conclusions

The early three-dimensional stages of ribbon-induced transition in a Blasius boundary layer were simulated numerically. The mean flow was treated as parallel and the disturbances as spatially periodic and time-developing. The concurrent growth of the boundary-layer thickness, the two-dimensional wave amplitude, and the three-dimensional disturbance amplitude was reproduced. The numerical periods and the type of disturbances were chosen to influence the physical processes as little as possible. Tests were conducted to rule out a strong dependence on numerical parameters.

The results are in agreement with Craik's analysis for low TS-wave amplitude, and with Herbert's analysis for all amplitudes. The agreement with Saric *et al.*'s (1984) experiments is good at low amplitudes, but only fair at higher amplitudes. For a given amplitude, the numerical results tend to agree with experimental results corresponding to lower amplitudes. The disagreement is at least partly explained by differences in the three-dimensional excitation of the boundary layer, even though in both cases it had a random character. This illustrates again the extreme sensitivity of transitional phenomena in Blasius flow. It suggests that further study of these fine effects should focus on devising the most credible procedure to input disturbances.

The authors thank Dr A. Wray (NASA Ames Research Center) for reviewing the manuscript, and Professor H. Reed (Arizona State University) and J. Ferziger (Stanford University) for useful discussions. The second author was supported by the AFOSR under grant 84-0083.

REFERENCES

Craik, A. D. D. 1971 Nonlinear resonant instability in boundary layers. *J. Fluid Mech.* **50**, 393–413.

Gaster, M. 1962 A note on the relationship between temporally increasing and spatially increasing disturbances in hydrodynamic stability. *J. Fluid Mech.* **14**, 222–224.

Herbert, Th. 1984 Analysis of the subharmonic route to transition. *AIAA* 84-0009.

Herbert, Th. 1985 Three-dimensional phenomena in the transitional flat-plate boundary layer. *AIAA*-85-0489.

Kachanov, Y. S. & Levchenko, V. Y. 1984 The resonant interaction of disturbances at laminar–turbulent transition in a boundary layer. *J. Fluid Mech.* **138**, 209–247.

Klebanoff, P. S., Tidstrom, K. D. & Sargent, L. M. 1962 The three-dimensional nature of boundary layer instability. *J. Fluid Mech.* **12**, 1–34.

Kleiser, L. & Laurien, E. 1985 Three-dimensional numerical simulation of laminar–turbulent transition and its control by periodic disturbances. In *Laminar–Turbulent Transition, Proc. 2nd IUTAM Symp., Novosibirsk* (ed. V. V. Kozlov), Springer.

Kovasznay, L. S. G., Komoda, H. & Vasudeva, B. R. 1962 Detailed flow field in transition. In *Proc. 1962 Heat transfer and Fluid Mechanics Institute*, pp. 1–26. Stanford University Press.

Laurien, E. & Kleiser, L. 1985 Active control of Tollmien–Schlichting waves in the Blasius boundary layer by periodic wall suction. In *Proc. 6th GAMM Conf. on Numerical Methods in Fluid Dynamics, Göttingen, Sept. 25–27, 1985*. Vieweg.

Orszag, S. A. & Kells, L. C. 1980 Transition to turbulence in plane Poiseuille and plane Couette flow. *J. Fluid Mech.* **96**, 159–205.

Saric, W. S., Kozlov, V. V. & Levchenko, V. Y. 1984 Forced and unforced subharmonic resonance in boundary-layer transition. *AIAA* 84-0007.

Schlichting, H. 1979 *Boundary layer theory*, 7th edn. McGraw-Hill.

SPALART, P. R. 1984 Numerical simulation of boundary-layer transition *9th Intl Conf. on Numerical Methods in Fluid Dynamics, Paris, June 25–29, 1984* (ed. S. Soubbaramayer & J. P. Boujot), pp. 531–535. Springer.

SPALART, P. R. 1986 Numerical simulation of boundary layers: Part 1. Weak formulation and numerical method. *NASA T. M.* 88222.

THOMAS, A. S. W. 1983 The control of boundary-layer transition using a wave-superposition principle. *J. Fluid Mech.* **137**, 233–250.

WRAY, A. & HUSSAINI, M. Y. 1980 Numerical experiments in boundary-layer stability. *AIAA paper* 80-0275 (see also *Proc. R. Soc. Lond.* A **392**, 373–389).

ZANG, T. A. & HUSSAINI, M. Y. 1985*a* Numerical experiments on subcritical transition mechanisms. *AIAA* 85-0296.

ZANG, T. A. & HUSSAINI, M. Y. 1985*b* Numerical experiments on the stability of controlled shear flows. *AIAA* 85-1698.